Forschung im Ingenieurwesen (2023) 87:833–844
https://doi.org/10.1007/s10010-023-00676-5

ORIGINALARBEITEN/ORIGINALS

Analytical method for calculating the nominal tooth root stress in worm gear shafts

Johannes Gründer[1] · Alexander Monz[1]

Received: 10 March 2023 / Accepted: 18 May 2023 / Published online: 21 June 2023

Abstract
According to the state of the art, worm gears are designed due to the softer bronze-material of the worm wheel primarily against damage of the wheel because of wear, pitting or breakage of the teeth. The aim of research in the last decades is to optimize the load capacity on the worm wheel by using higher-strength bronze alloys, cast iron or steel to increase the transmission capacity of worm gears. This development may lead to an increased number of damage cases on the worm shaft. In literature, documented cases of tooth segment fractures of the worm shaft can already be found. Since the worm is only designed against deflection according to the state of the art, there is a need for a method to calculate the material stress in worm shafts. This paper presents an analytical method based on the nominal stress approach for calculating bending, compression, and shear stresses in the tooth root of worm shafts to close this gap. The stresses resulting from different load distributions in the tooth contact due to assembly deviations are calculated with the presented method and compared with results from the Finite Element Method.

Analytische Methode zur Berechnung der Nennspannungen im Zahnfuß von Schneckenwellen

Zusammenfassung
Schneckengetriebe werden nach dem Stand der Technik aufgrund des deutlich weicheren Bronze-Werkstoffes primär auf Seite des Schneckenrades gegen Verschleiß, Grübchenbildung und Zahnfußbruch des Rades ausgelegt. Ziel der Forschung ist daher häufig die Lastoptimierung der Schneckenräder durch den Einsatz von höherfesten Bronze-Legierungen, Gusseisen oder Stahl zur Steigerung der übertragbaren Leistung der Schneckengetriebe. Dadurch wird potenziell die Leistungsgrenze der Getriebe in einigen Betriebsbereichen hin zur Schneckenwelle verschoben. In der Literatur finden sich bereits dokumentierte Fälle von Zahnbrüchen an der Schneckenwelle. Da die Schneckenwelle nach Stand der Technik nur gegen Durchbiegung ausgelegt wird ergibt sich die Notwendigkeit einer Methode zur Berechnung der Materialbeanspruchung in Schneckenwellen. In dieser Arbeit wird eine analytische Methode auf Basis des Nennspannungsansatzes zur Berechnung von Biege-, Druck- und Schubspannungen im Zahnfuß von Schneckenwellen vorgestellt. Die aus verschiedenen Lasttragbildern resultierenden Spannungen werden mit der vorgestellten Methode berechnet und mit Ergebnissen der Finiten Elemente Methode verglichen.

1 Tooth fracture on worm shafts

Worm gears are helical gear units with an axis cross angle of 90° and are characterized by large gear ratios in one gear stage, high transmissible torques and smooth-running properties. Due to the high sliding ratio and the high temperatures occurring in tooth contact, the worm shaft is usually made of case-hardened steel and the worm wheel of a copper-tin alloy to avoid scuffing damage. The design of worm gears is primarily carried out on the side of the wheel to prevent excessive wear and pitting of the tooth flanks as well as tooth fracture due to the softer material. The worm shaft on the other hand is designed according to the state of the art in DIN 3996 [1] and ISO/TS 14521 [2] only against deflection to prevent displacements of the contact pattern

✉ Johannes Gründer
johannes.gruender@th-nuernberg.de

[1] Institute for Chemistry, Materials and Product Development (OHM-CMP), Nuremberg Institute of Technology, Keßlerplatz 12, 90489 Nuremberg, Germany

and increase of local loads on the tooth flanks [1, 3]. Further investigations in [4, 5] aim to improve this calculation method. In ANSI/AGMA 6022-C93 [6], an additional design aspect provides the calculation of the bending stress in the worm shaft with a highly simplified approach.

Addressing the damage on worm shafts, only the formation of scores and cracks on the tooth flank surfaces is studied in detail in [7, 8]. However, fractures of the worm teeth are observed in various research projects [9–13] as side effect during other investigations. Photographs of the damages as documented in the literature are shown in Fig. 1. The fractures are attributed to low material quality in [9], to contamination with water in [11] and to the influence of inductive hardening of the worms' surface layer in [13]. In [10, 12], the damage is observed when operating with standard bronze and without unusual external influences.

Past and current efforts to enhance the wheel material by using higher strength bronze alloys [12] or to substitute bronze with cast iron [9, 14] and steel [15, 16] aim to increase the transmissible torque at the wheel. This development may lead to the strength of the worm shaft constraining the performance. To close this gap in the state of the art, the authors devote this paper to the development of a method for calculating the material stress in the tooth root of the worm shaft.

2 State of the art

For designing helical gears against fracture at the tooth root, the maximum local stress σ_F is usually compared with the tooth root stress limit σ_{FG} which is calculated from the permissible stress σ_{FP} by considering stress concentration, higher load capacity for a limited number of load cycles, notch sensitivity, surface roughness and the influence of the tooth dimensions on the tooth bending strength. According to ISO 6336-3 [17], it is assumed that exceeding the permissible bending stress results in damage of the gear. The safety factor S_F is calculated according to Eq. 1.

$$S_F = \frac{\sigma_{FG}}{\sigma_F} \geq S_{\mathrm{Fmin}} \tag{1}$$

The gearbox is assumed to be operated safely with S_F being equal to or greater than S_{Fmin}. In DIN 3990-1 [18] it is recommended to select the minimum safety factor S_{Fmin} depending on the accuracy of the used calculation method and specific for different applications. In ISO 6336-3 [17], the maximum local tooth root stress σ_F is obtained by multiplying the nominal tooth root stress σ_{F0} with various stress correction factors. The nominal tooth root stress σ_{F0} is calculated according to Eq. 2 by the ratio of the nominal tangential load F_t to the product of the facewidth b and the normal module m_n. Various influences on the bending stress such as the gears tooth form factor Y_F, the stress concentration factor Y_S, the factor Y_β for the irregular load distribution along the contact lines in helical gears, the rim thickness factor Y_B and the deep tooth factor Y_{DT} for high precision gears are additionally considered.

$$\sigma_{F0} = \frac{F_t}{b \cdot m_n} \cdot Y_F \cdot Y_S \cdot Y_\beta \cdot Y_B \cdot Y_{DT} \tag{2}$$

When designing worm wheels according to DIN 3996 [1], the maximum shear stress τ_F is compared with the shear stress limit τ_{FG} from which a safety factor S_F is calculated. This method is also based on a nominal stress approach by obtaining τ_F from the ratio of the tangential force F_{tm2} to the product of the facewidth b_{2H} and the axial modulus m_x multiplied by similar stress correction factors.

The FKM guideline [19] offers a comprehensive calculation method for assessing the strength of components with any geometry under both static and dynamic load by performing in depth analysis with the Finite Element Method (FEM). Since this procedure is usually very time-consuming, it can only be applied to a small number of components with reasonable effort. The permissible stress of any component at the most stressed location depends on the material and the respective quality, the manufacturing process, the technological size, the surface roughness, the hardness of the component as well as the experienced load over time. Specific studies on the strength of worm shafts and the influences are hardly available. Reference values for the

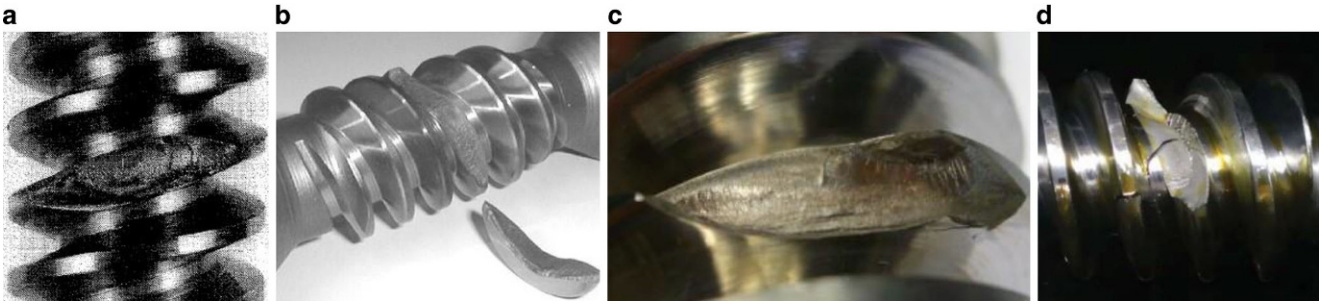

Fig. 1 Broken teeth on worm shafts due to overload. (From **a**–**d** [9–12])

roughness of the worm shaft are given in DIN 3996 [1] while detailed measurements are provided in [12, 20–22]. Data of measured surface hardness is found in [20, 22, 23]. At the current state of the art, the strength of worm shaft geometries cannot be determined.

2.1 Stress calculation in worm gears

According to ANSI/AGMA 6022-C93 [6], the design of worm shafts against deflection and bending stress is based on the model of a circular bending beam. The maximum bending stress S_b is compared with the permissible stress depending on the material. Stress concentrations in the worm thread due to the tooth rounding as well as the load distribution and the geometric influence on the worm shafts stiffness remains unattended.

The stress concentration in grooved shafts can be calculated using the method described in DIN 743-2 [24]. Due to the helical geometry of the worm thread, this method is not suitable for calculating the local bending stress.

To calculate the stress in the tooth root fillet, an approach based on the slice theory was formulated in [25]. Bending, compression and shear stresses are calculated in each loaded slice along the contact line. The method does not consider the distribution of stress in the tooth root under point load.

In experimental studies carried out in [26], the bending of the worm and wheel teeth were measured with an optical interferometer and an empirical equation for calculating the material stress in the tooth root based on the measurements was derived. The influence of deviation-related contact patterns on the tooth deformation and tooth root stress was investigated.

To calculate the tooth root stress in both worm and wheel, in [27] an approach based on the finite element method was developed. The calculations were performed with a constant line load to investigate the influence of geometry parameters on the stress and to approximate the distribution in the tooth root with equations.

Investigations of material stress in worm gears were carried out in [28, 29] for both the worm and the wheel teeth using FEM. The investigations were application-related and did not aim to develop a calculation method for the stress in the worm. Further investigations in [10, 30, 31] using FEM were focused exclusively on the material stress in the worm wheels.

2.2 Load distribution in worm gears

The load distribution in the tooth contact of worm gears depends on the contact points between the flanks. In ISO/TR 10828 [32], a method for calculating the contact lines in unloaded condition is presented. The basis for the Software SNETRA by the German Research Association for Drive Trains (FVA) for calculating load patterns under load was provided in [33]. By simulating the manufacturing process and considering assembly deviations, the load distribution can be predetermined during the design process. The analytical approximation of the stiffness matrix of all contact points allows the time-efficient calculation of a wide variety of different geometric parameters. The availability of the contact load distribution is the basic requirement for calculating the material stresses in the bodies.

2.3 Stress calculation in helical spur gears

An extended calculation approach for the tooth root stress in helical spur gears based on DIN 3990-3 [34] was developed in [35] by considering the load distribution on the tooth flanks and the supporting effect of the unloaded width of the tooth. The distribution of the bending stress in the tooth root is calculated using approximate equations developed in [36] based on numerical investigations of straight cantilever plates.

3 General stress in worm shafts

Worm shafts experience various types of stress during operation. On the one hand, stresses occur in the tooth root due to the load transmission like a helical spur gear. The stress distribution in the tooth root is different due to the curvature of the teeth around the worm shaft axis and the constant supporting effect of the teeth on both sides of the contact line due to the continuous helical geometry. On the other hand, bending stresses occur in the tooth gap of the worm, since it is usually designed with a large distance between the bearings and relatively small diameters. Because of the helical geometry of the tooth gap, the stress cannot be calculated according to DIN 743-2 [24] since there is no similar groove provided. According to [37], the tooth root of external gears experience bending, compression and shear. The stress in the tooth root and in the cross section of the shaft is shown schematically in Fig. 2.

The ability to accurately calculate stress in worm shafts offers the potential to derive a simplified yet validated calculation method. First, the stresses in the tooth root of a worm shaft with standard reference geometry according to DIN 3996 [1] and DIN 3975-1 [38] are calculated at a defined operating point for a deviation-free toothing using FEM. The gearing and load data of the investigated geometry as well as the contact pattern including the lines of contact and the load distribution as calculated with SNETRA [33] are summarized in Table 1. The load distribution on several tooth flanks due to the overlap ε is already considered in the contact pattern calculation.

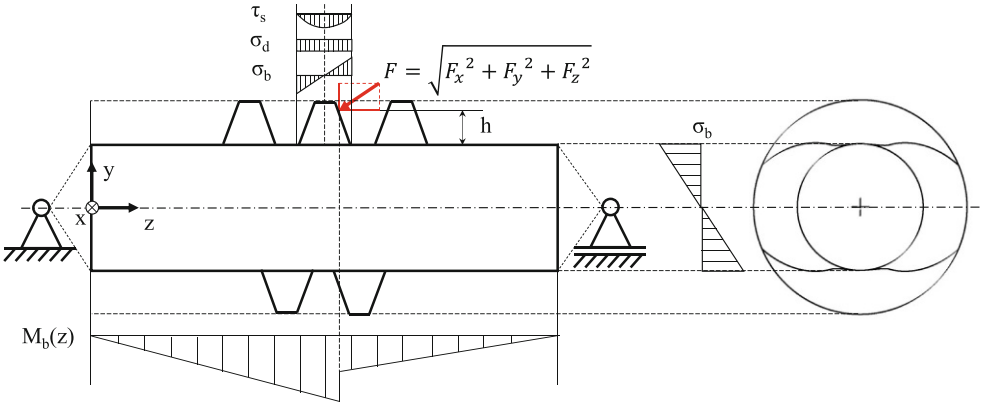

Fig. 2 Schematic stress in the tooth root and in the transverse section of a worm shaft

Table 1 Gear geometry, load data, contact lines and load distribution on the tooth flanks as calculated with SNETRA

Variable	Unit	Value	Material data, load data and load distribution		
a	*[mm]*	100	Material Worm, Wheel	*[–]*	16MnCr5/CuSn12-C-GZ
z_2/z_1	*[–]*	41/2	E_1/E_2	$[N/mm^2]$	210,000/98,100
q	*[–]*	9	υ_1/υ_2	*[–]*	0.3/0.35
M_x	*[mm]*	4	T_2	*[Nm]*	1350
α_0	*[°]*	20	n_1	*[rpm]*	60
r_{f1}	*[mm]*	1.52	*Line load F*	*[N/mm]*	150 … 500
H_f*	*[–]*	1.25	$\sigma_{H,max}$	$[N/mm^2]$	694,54
h_a*	*[–]*	1.00			
b_1	*[mm]*	65			
b_2	*[mm]*	30			
l_1	*[mm]*	160			

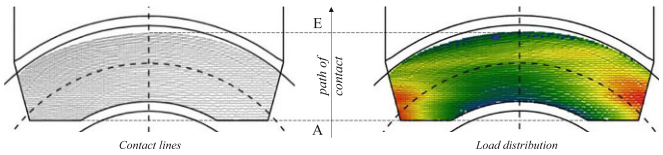

3.1 FEM-Model for calculating the stress in the tooth fillet

To build the FEM model, a toothed segment of the worm shaft is separated and clamped with a fixed support at the cut surfaces. The load is applied along an imprinted contact line on the tooth flank according to the calculated load distribution as seen in Table 1. For this purpose, the line load F as calculated with SNETRA is converted to n point loads for every node along the contact line in the FEM. Assuming that contact forces are always acting normal to the contact surface, the line load F is divided into its components F_x, F_y and F_z by calculating the direction of the normal vector in each point along the contact line. The FEM model is shown in Fig. 3.

The model is solved for 10 equally distributed contact lines of the contact pattern as shown in Table 1, starting with the line in point A of the first contact. The evaluation of the results is further carried out in the point of the maximum principal stress σ_1. The components of the stress tensor s are evaluated along paths intersecting this point in the circumferential (path β), the tooth root rounding (path β_{rf1}) and the normal direction into the component (path t) as shown in Fig. 3. The maximum principal stress σ_1 resulting from passing through the entire contact pattern is shown in Fig. 4. It can be observed that the maximum stress is not caused by either the largest lever arms when contact happens at the tip diameter, or the largest line loads near the root diameter. Fig. 5, 6 and 7 show the evaluated stress components along the paths as defined in Fig. 3.

According to Fig. 5, the normal stresses σ_y and σ_z and the shear stress τ_{xy} represent the dominant components. The maximum bending stress $\sigma_{y,max}$ occurs in the tooth root radius at $\beta_{rf1} = 60°$ as seen in Fig. 6 which corresponds to the assumption of the location at the $30°$ tangent according to ISO 6336-3 [17]. The maximum of all stress components

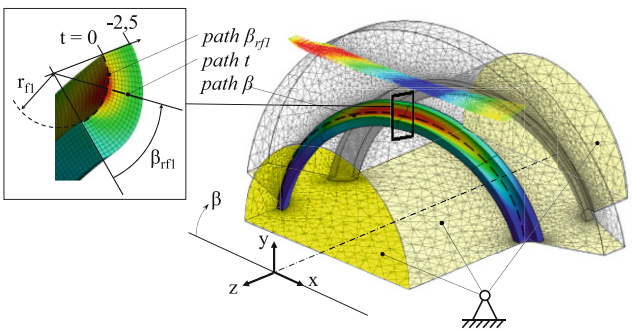

Fig. 3 FEM-Model for calculating the stress distribution in the tooth root under line load

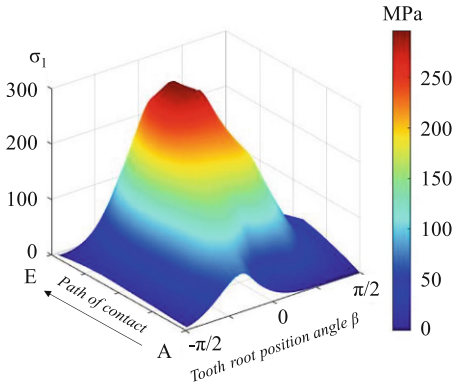

Fig. 4 Distribution of the maximum principal stress σ_1 in the tooth root as calculated with FEM for 10 contact lines of the contact pattern shown in Table 1

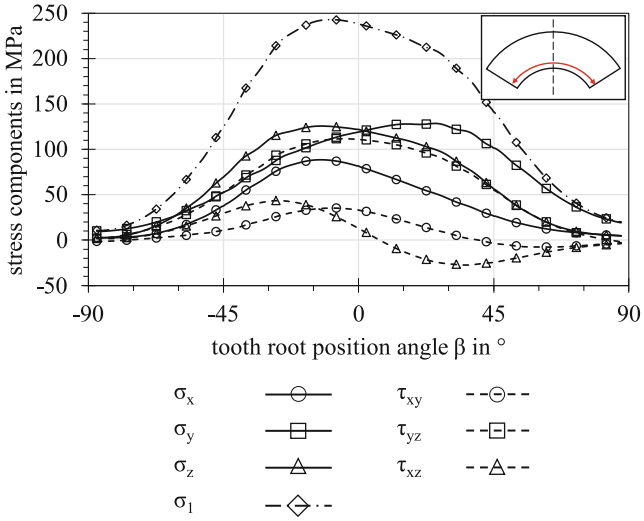

Fig. 5 Stress components calculated with FEM along path β

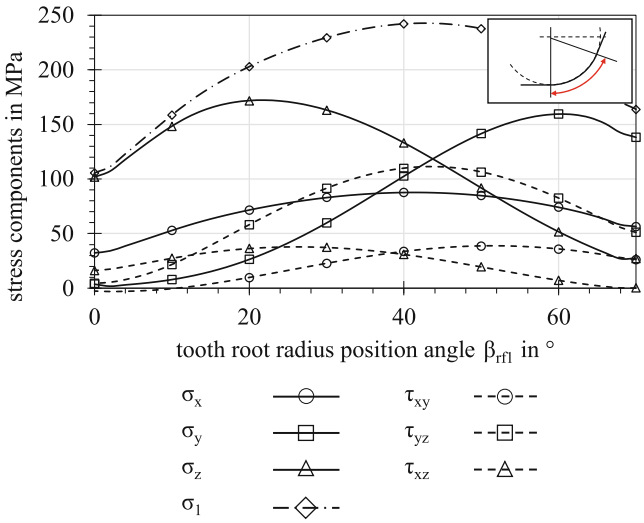

Fig. 6 Stress components calculated with FEM along path β_{rf1}

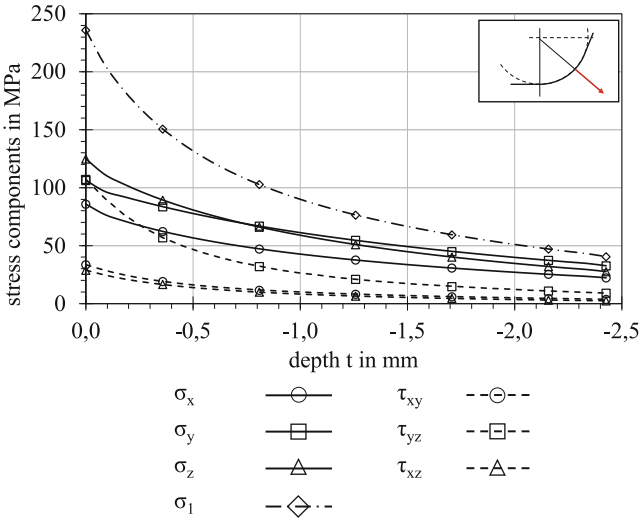

Fig. 7 Stress components calculated with FEM along path t

is located at the surface of the tooth rounding where $t = 0$ as seen in Fig. 7. Therefore, only the stress at the surface is considered in the following elaboration.

4 Analytical calculation model

To calculate the stress in the tooth root of worm shafts, an initial approach based on the calculation of the nominal stresses following the method according to ISO 6336-3 [17], DIN 3990-3 [34] and the extended calculation method in [35] is presented. Further, equations for the calculation of the nominal bending, compression and shear stresses in the tooth root are derived. The calculation model is based on the discretization of the line load F along each contact line. The stress distributions resulting from each individual point load F_i are summarized to calculate the total stress distribution in the worm tooth root. The method is shown in Fig. 8.

The dismantling of the point load F_i into its components $F_{x,i}$, $F_{y,i}$ and $F_{z,i}$ at any point $P_{F,i} = (x_i \mid y_i \mid z_i)$ along the contact line is performed by obtaining the direction of the normal vector $n_{P,i}$ at $P_{F,i}$ on the surface of the flank. The force vector components $F_{x,i}$ and $F_{y,i}$ need to be rotated in every point $P_{F,i}$ by the position angle $\beta_{F,i}$ so that $F_{x,i}'$ points in tangential and $F_{y,I}'$ in radial direction. The force components are rotated according to Eqs. 3 and 4.

$$F_{x,i}' = F_{x,i} \cdot \cos\left(\beta_{F,i}\right) - F_{y,i} \cdot \sin\left(\beta_{F,i}\right) \tag{3}$$

$$F_{y,i}' = F_{y,i} \cdot \cos\left(\beta_{F,i}\right) + F_{x,i} \cdot \sin\left(\beta_{F,i}\right) \tag{4}$$

The force component F_z always points in axial direction and does not need to be converted. Figure 9 shows the rotation of the force components of a single point load F_i

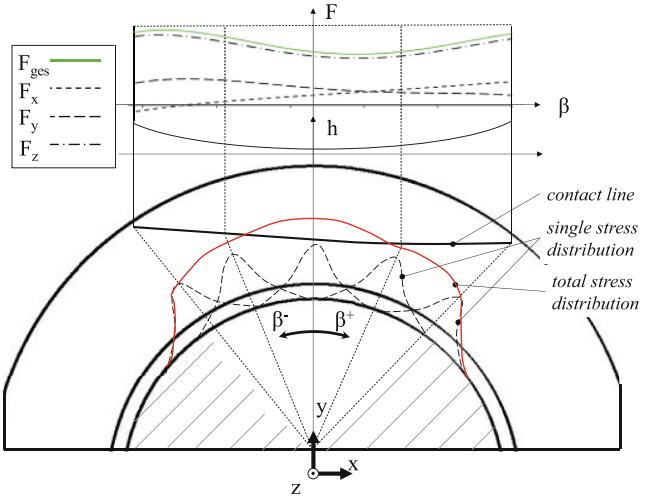

Fig. 8 Calculation model for discrete load application and stress distribution

in point $P_{F,i}$. The radius r_i of the force application point corresponds to the distance of the point $P_{F,i}$ to the worm axis.

Equations are formulated for the types of loads in the tooth root of the meshing flank of an external gear according to [37]. The calculation of the nominal stress is based on a worm shaft with ZA flank profile and geometry according to DIN 3975-1 ([38], see Fig. 10).

Following DIN 3990-3 [34], the nominal bending stress $\sigma_{b,nom}$ is related to the tooth thickness $s_{f\gamma}$ at the root circle diameter d_{f1} in the effective direction of the forces F_x' and F_y' at the angle γ_F.

The tooth thickness s_{fx} in the axial section is determined approximately according to Eq. 5.

$$s_{fx} = s_{mx} + tan\,(\alpha_0) \cdot \left(d_{m1} - d_{f1}\right) \tag{5}$$

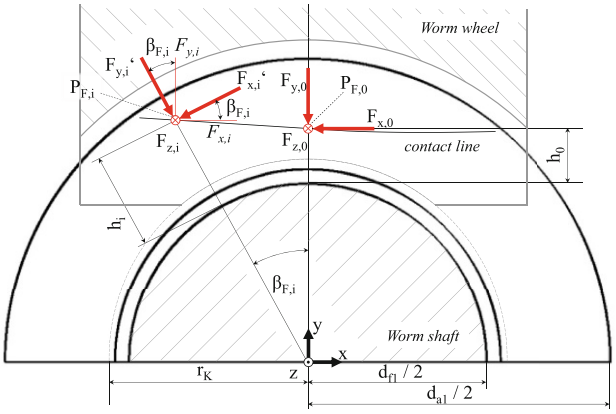

Fig. 9 Load application in the calculation model

The tooth thickness $s_{f\gamma}$ is calculated for every force application point by Eq. 6.

$$s_{f\gamma} = s_{fx} \cdot cos\left(arctan\left(\frac{F_x'}{F_z}\right)\right) \tag{6}$$

To calculate the bending Moment M_b, the effective lever arm h_{Fe} is adopted from DIN 3990-3 [34] and modified for the worm geometry. It represents the distance between d_{f1} and the point of intersection of the centre of the tooth with the force line resulting from F_y' and F_z in the axial section. The effective lever arm is calculated according to Eq. 7.

$$\begin{aligned} h_{Fe} = r_i - \frac{d_{f1}}{2} - \tan\left(\arctan\left(\frac{F_y'}{F_z}\right)\right) \cdot s_{fx} \\ + \tan\left(\alpha_0\right) \cdot \left(\frac{d_{m1}}{2} - r_i\right) \end{aligned} \tag{7}$$

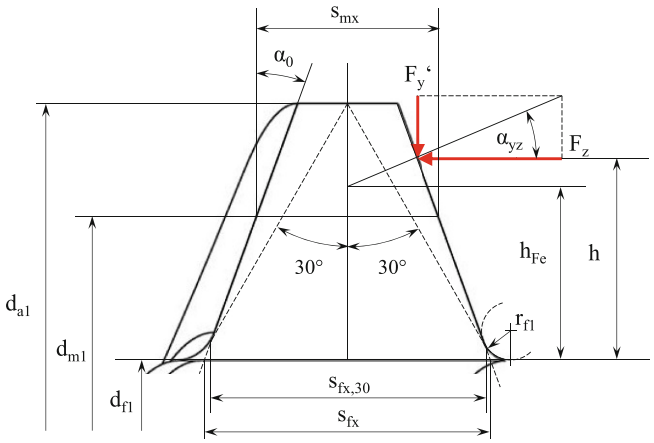

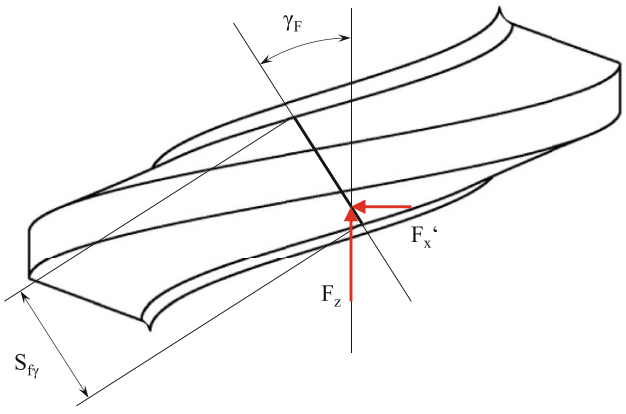

Fig. 10 Geometric parameters of the worm shaft tooth with ZA flank profile

The nominal bending stress $\sigma_{b,nom}$ resulting from the tangential and axial force components F_x' and F_z is calculated according to Eq. 8.

$$\sigma_{b,\mathrm{nom}} = \frac{M_b}{W_b} = \frac{\sqrt{F_x{}'^2 + F_z{}^2} \cdot h_{Fe}}{\frac{s_{f\gamma}{}^2}{6}} \tag{8}$$

The nominal compressive stress $\sigma_{d,nom}$ is calculated using the radial force F_y' according to Eq. 9 and is related to the tooth thickness s_{fx} at the root diameter in the axial section.

$$\sigma_{d,\mathrm{nom}} = \frac{F_d}{A} = \frac{F_y{}'}{s_{fx}} \tag{9}$$

The nominal shear stress $\tau_{s,nom}$ is calculated from the forces in tangential and axial directions F_x' and F_z in relation to the tooth root thickness s_{fy} at the root circle diameter d_{f1} in the direction of the force according to Eq. 10.

$$\tau_{s,\mathrm{nom}} = \frac{F_s}{A} = \frac{\sqrt{F_x{}'^2 + F_z{}^2}}{s_{f\gamma}} \tag{10}$$

4.1 Numerical calculation of the distribution of force and moment on a curved plate

To calculate the nominal stress, the distribution of the bending moment as well as the reaction forces at the root of the tooth need to be considered. For this purpose, numerical simulations using FEM are carried out on a plate model according to [36] but with modified geometry. The presented plate geometry corresponds to the standard reference geometry of a worm shaft according to DIN 3996 [1] and DIN 3975-1 [38]. The plate is located at the centre of the worm tooth segment and is loaded with a point load $F = 1\,N$ at the point $P_F = (x_F \mid y_F \mid z_F)$. The lever arm h is the distance of the point P_F to the clamping at the root circle diameter. The model is shown in Fig. 11.

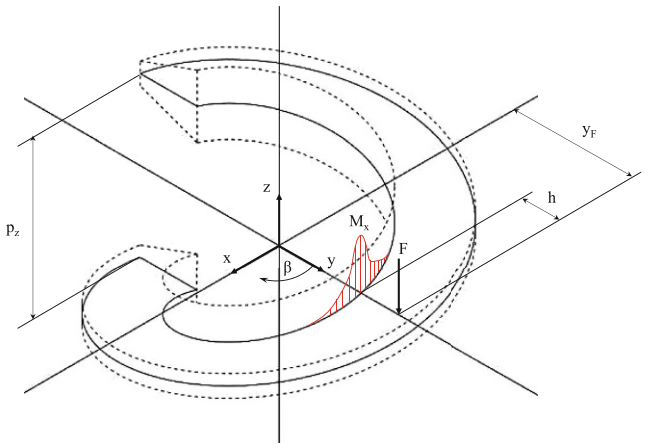

Fig. 11 Modified curved plate with worm shaft geometry

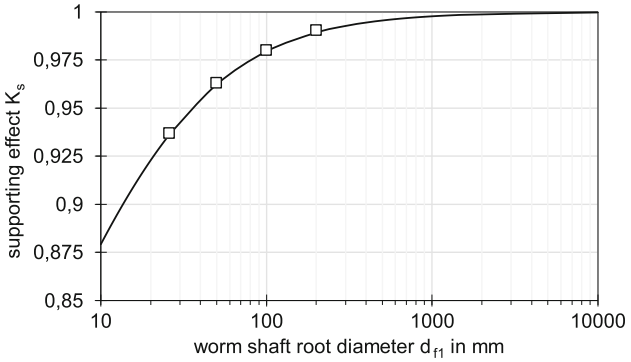

Fig. 12 The Supporting effect of curved plates

The response variables M_x, F_y and F_z are distributed at the clamping under load. The integral of the distribution of the reaction moment is equal to the product of force F and lever arm h. The curvature of the plate compared to the model of a straight spur gear tooth reduces the reaction moment in the tooth root due to the supporting effect of the non-loaded areas of the worm. The support factor of the curved geometry is considered via the function K_S. The reaction moment is calculated according to Eq. 11.

$$\int M_b = F \cdot h \cdot K_S \tag{11}$$

To determine the supporting effect K_S, the root circle diameter d_{f1} of the plate is varied up until the curvature is equal to a uncurved plate for $Fz = 1\,N$ and $h = 0.9$. The values are calculated from the difference of the nominal moment and the integral of the reaction moment of the numerical solution.

The increase of the supporting effect with decreasing diameter and thus the reduction of the bending moment is shown in Fig. 12. The function K_S is approximated by Eq. 12.

$$K_S = f\left(q, {h_{f1}}^*, {h_{a1}}^*\right) = \left(\frac{q - 2 \cdot {h_{f1}}^*}{q + 2 \cdot {h_{a1}}^*}\right)^{0{,}125} \tag{12}$$

Figure 13 shows the model of a straight tooth with a contact line that does not extend over the entire width of the flank. According to [35], the length and position of the contact line change the distribution of the bending moment. When analysing the worm geometry, no case distinction is necessary since there are always identical supporting widths to both sides of the contact line for each possible position on the worm flank as well as no free-standing tooth ends.

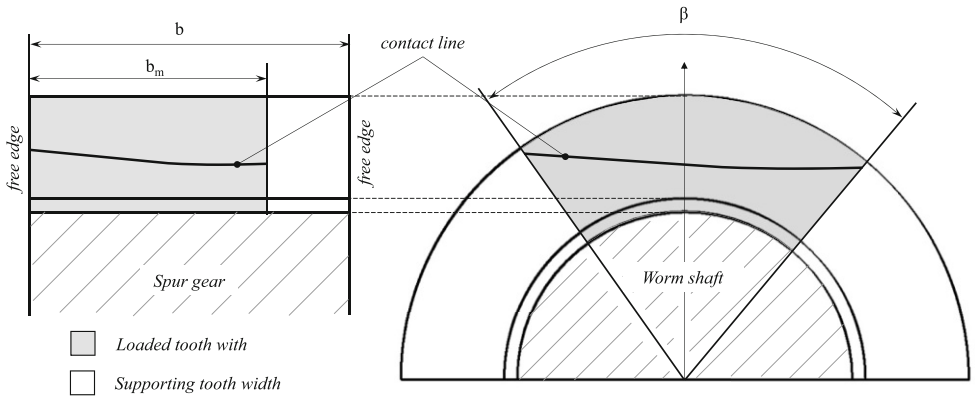

Fig. 13 Supporting and non-supporting tooth width on helical gear and worm shaft

4.2 Approximate function for the distribution of force and moment

The force and moment distributions on the curved plate are approximated with the equation of the standard normal distribution. The distribution function D is defined in Eq. 13.

$$D = f\left(\beta, \beta_F, p_1, p_2\right) = p_1 \cdot e^{\left(-\left(\frac{\beta-\beta_F}{p_2}\right)^2\right)} \tag{13}$$

In function D, the parameter p_1 resembles the maximum value, p_2 the opening width and β_F the angular position of the force application point according to Fig. 9. The distributions resulting from the numerical plate model are evaluated as an example for the bending moment D_{Mx} (see Fig. 14) and the shear force D_{Fz} (see Fig. 15) under load with $F = 1\,N$ and different lever arms h. The lever arm h is normalized with d_{f1} corresponding to *0* and d_{a1} to *1*.

The change of the parameters p_1 and p_2 of the distribution function D depending on the lever arm h are approximated with 2nd degree polynomials with the parameters k_1, k_2 and k_3 according to Eq. 14.

$$p_{1,2} = k_1 \cdot h^2 + k_2 \cdot h + k_3 \tag{14}$$

The variation of the parameters p_1 and p_2 depending on the lever arm h is shown in Fig. 16 for the moment distribution D_{Mx} and in Fig. 17 for the axial reaction force distribution D_{Fz}.

5 Calculation of the stress distribution

The individual stress distribution $\sigma_{b,nom,D,i}$ in the tooth root resulting from each individual load F_i along a contact line of the contact pattern is calculated according to Eq. 15. using Eqs. 8, 12 and 13.

$$\sigma_{b,\mathrm{nom},D,i} = \frac{M_{b,i}}{W_{b,i}} \cdot K_S \cdot D_{b,i} \tag{15}$$

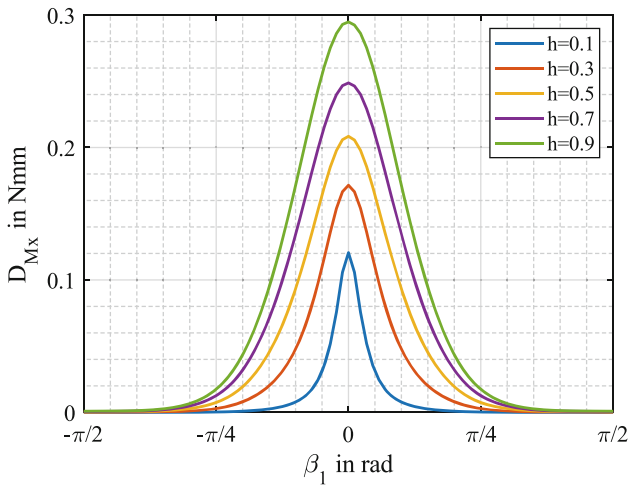

Fig. 14 Distribution of the moment reaction M_x in the tooth root calculated with the plate model

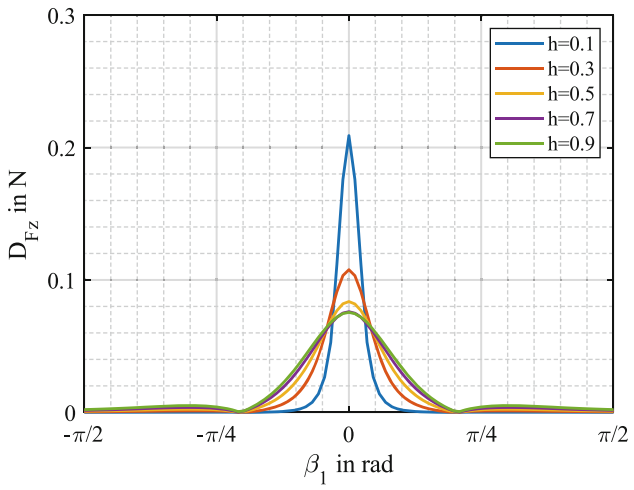

Fig. 15 Distribution of the force reaction F_z in the tooth root calculated with the plate model

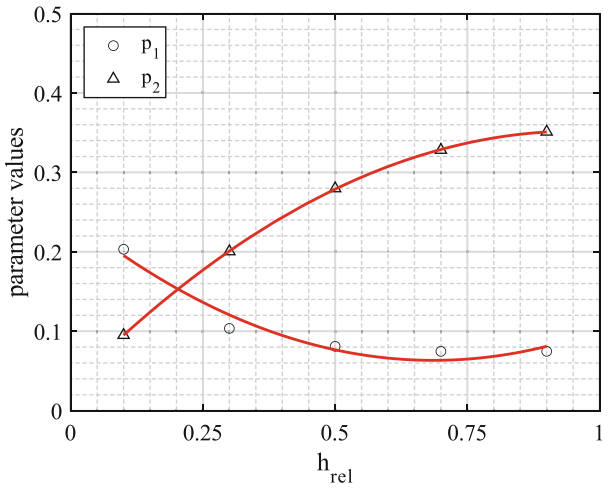

Fig. 16 Parameters *p1* and *p2* of the moment distribution function D_{Mx}

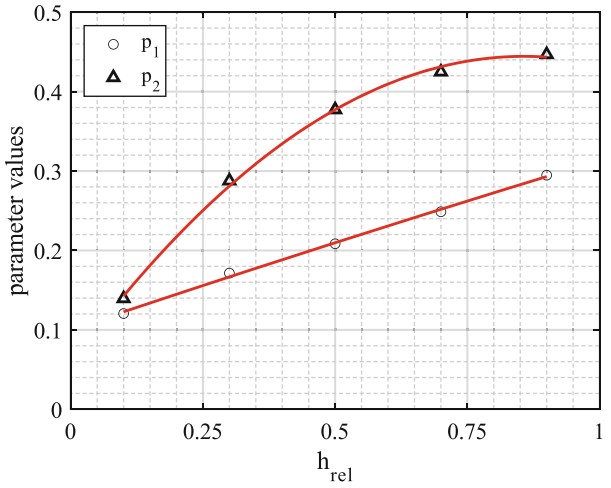

Fig. 17 Parameters *p1* and *p2* of the force distribution function D_{Fz}

The total stress distribution $\sigma_{b,nom,D}$ is calculated by superimposing the single distributions $\sigma_{b,nom,D,i}$ for one contact line according to Eq. 16.

$$\sigma_{b,\mathrm{nom},D} = \sum \sigma_{b,\mathrm{nom},D,i} \tag{16}$$

The stress distributions are calculated for the gear geometry and load as shown in Table 1. The calculation is performed for a deviation-free assembly, a displaced worm in axial direction by $\Delta a = -0.2\,mm$ and a displacement in width direction by $\Delta b = -0.2\,mm$ as defined in [33]. The load patterns calculated with SNETRA are shown in Fig. 18.

Applying the presented calculation method, the results of the nominal stress components $\sigma_{b,nom}$, $\sigma_{d,nom}$ and $\tau_{s,nom}$ for each contact pattern are shown in Fig. 19. Since the stress concentration in the tooth root rounding is not considered, all stress components are normalized for comparison to the respective maximum value of the deviation-free assembly. The normalisation is carried out exemplarily for the bending stress $\sigma_{b,norm}$ according to Eq. 17. Although the stress concentration effect in the worm tooth root rounding is not included in the calculation, the amount of increase of the stress level caused by assembly deviations is expected to be accurate. It is observed that the contact patterns of the deviating assemblies do impact the maximum values of the stress components with the shear stress being the most affected with an increase of up to *72%*.

$$\sigma_{b,\mathrm{norm}} = \frac{\sigma_{b,\mathrm{nom}}}{\max\left(\sigma_{b,\mathrm{deviation-free}}\right)} \tag{17}$$

6 Validation and discussion

As shown in Fig. 20, the analytical calculated bending stress distribution for $\sigma_{b,nom}$ is corresponding with the FEM-results for the stress component σ_y when compared qualitatively, although the contours of the distributions differ slightly. Since the stress concentration is not considered, all stress values are normalized to the respective maximum value. The reason for the divergence is due to the stress component σ_y from the FEM calculation being similar to the bending stress due to its direction on the worm tooth root but does not correspond exactly to the same value. It is not possible to determine the amount of bending stress in the 3D FEM analysis because of the complex triaxial stress state.

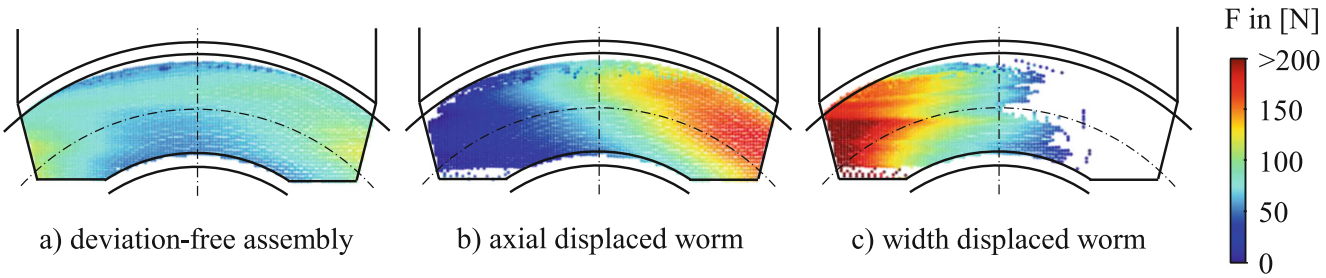

Fig. 18 Calculated load distributions *F* using SNETRA of the standard reference geometry under load with $T_2 = 1350\,Nm$ and $n_1 = 60\,rpm$. The point loads in the contact patterns are shown for a) deviation-free assembly, b) axial displaced worm ($\Delta a = -0.2\,mm$) and c) width displaced worm ($\Delta b = -0.2\,mm$)

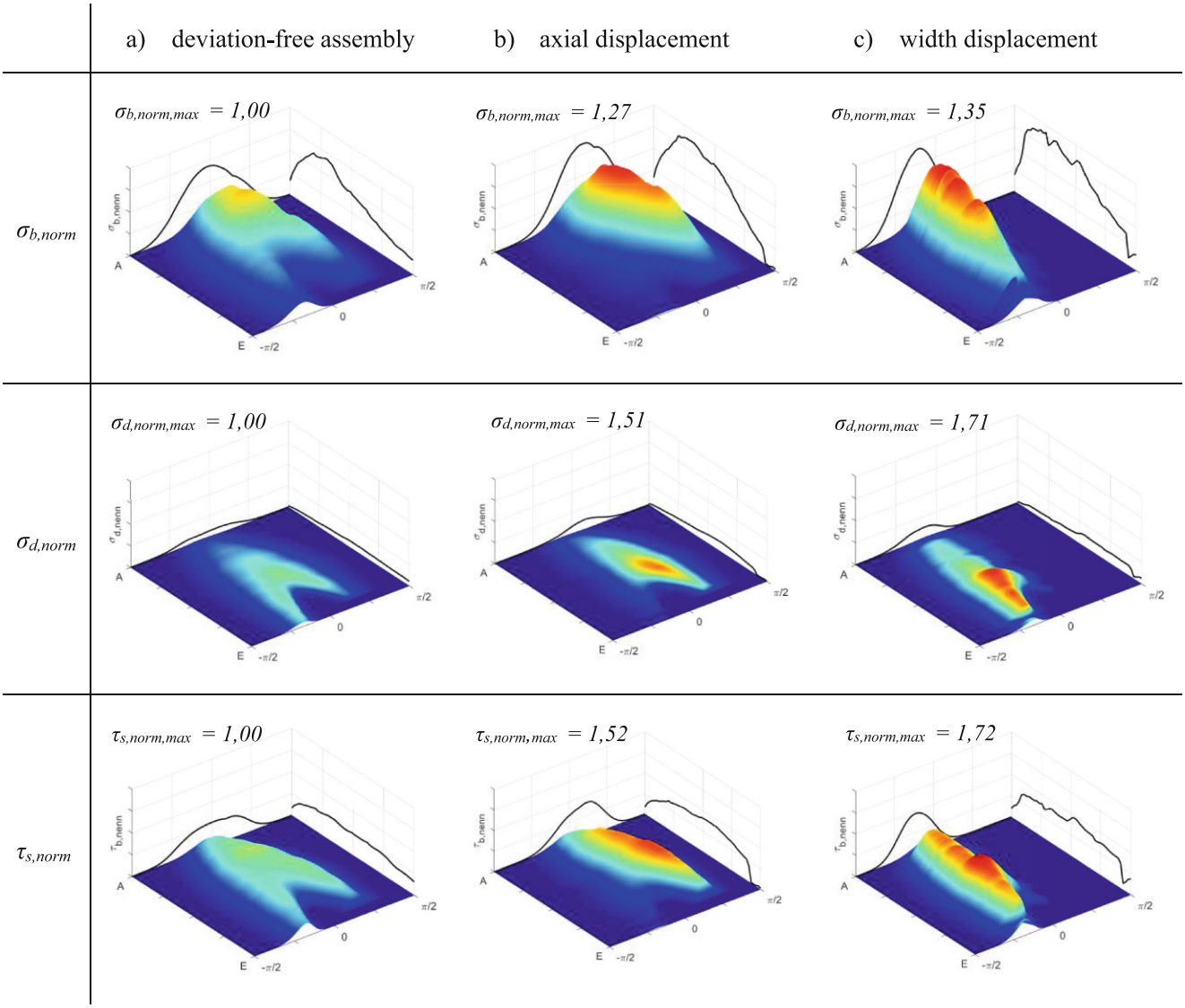

Fig. 19 Calculated nominal bending stress $\sigma_{b,nom}$, nominal compressive stress $\sigma_{d,nom}$ and nominal shear stress $\tau_{s,nom}$ for the contact patterns calculated with SNETRA: a) deviation-free assembly, b) axial displaced worm and c) width displaced worm. All values of the stress components are normalized to the corresponding max. value of the deviation-free assembly

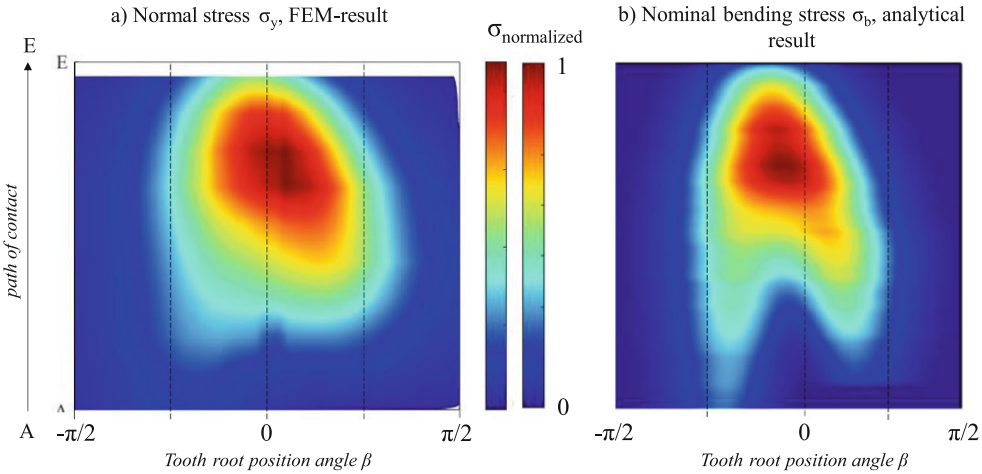

Fig. 20 Comparison between the distribution of a) the normalized normal stress component σ_y calculated with FEM and b)the normalized bending stress component $\sigma_{b,nom}$ calculated with the analytical method

7 Summary and conclusion

The presented calculation method allows design engineers do determine the expected nominal stress in the tooth root of worm shafts based on the load distribution in the tooth contact. The results show qualitatively good accuracy compared to the results calculated with FEM while the calculation time becomes faster and thus more efficient. This enables a fast and easy comparison of the stress overload between different worm geometries for different operating points. However, at the current stage of development, no statement about the actual stress values is possible since the stress concentration effect of the tooth root rounding is not considered. In addition, the lack of experimental data of permissible stresses of the worm shaft geometries does not allow to calculate the proof of strength.

The subject of future investigations can therefore be the stress concentration effect occurring in worm tooth root rounding by either specific calculation using FEM or adaptation of existing values in accordance with ISO 6336 [17] and DIN 3990-3 [34]. To provide a strength verification, the location experiencing the highest stress value is required. Since the worm is rotating and the locations along the shaft are stationary with respect to the axis position, it is not possible to directly identify a main stressed location from the presented calculation results. It is conceivable to derive periodic stress curves of the individual locations along the worm shaft. Like the stress concentration effect in the root of the worm shaft, the stress concentration of the helicoidal tooth space experiencing bending stress remains unknown. The adaptation of the method according to DIN 743-2 [24] in combination with the determination of new stress concentration factors for helical grooves offers potential. Finally, experimental investigations of the permissible stresses of different worm shaft geometries, both under load in the tooth contact area as well under bending stress, are necessary to calculate the strength of worm shafts.

8 Nomenclature

The nomenclature is shown in Table 2.

Table 2 Symbols

a	Centre distance *[mm]*
b_1, b_2	Worm thread width, wheel width *[mm]*
d_{a1}, d_{f1}, d_{m1}	Diameters of the worm shaft *[mm]*
h, h_{Fe}	Lever arm and effective lever arm *[mm]*
h_{a1}*, h_{f1}*	Worms tooth height factors *[–]*
k_1, k_2, k_3	Coefficients of parameter functions *[–]*
l_1	Bearing distance of the worm *[mm]*
M_x, m_n	Axial modulus, normal modulus *[mm]*
n_1	Rotational speed of the worm *[rpm]*
p_1 ,p_2	Parameters of distribution functions *[–]*
q	Form factor *[–]*
r	Radius of the force application point*[mm]*
r_{f1}	Tooth root radius
$S_{fn\,/fx/f\gamma/mx}$	Tooth widths of the worm *[mm]*
t	Depth coordinate *[mm]*
x, y, z	Cartesian coordinate directions *[mm]*
z_1, z_2	Number of threads of the worm and teeth of the worm wheel *[–]*
A	Surface area *[mm²]*
	Start point of the contact path *[–]*
D	Distribution functions *[–]*
E	End point of the contact path [–]
E_1, E_2	Youngs modulus of worm and wheel *[N/mm²]*
F	Point force *[N]* or line load *[N/mm]*
K_S	Support effect function *[–]*
M_b	Bending moment *[Nm]*
P_F	Force application point *[–]*
T_2	Moment on the worm wheel *[Nm]*
S_F	Safety factor against tooth fracture *[–]*
S_{Fmin}	Minimum safety factor *[–]*
W_b	Section modulus *[mm³]*
Y_F, Y_S, Y_β, Y_B, Y_{DT}	Tooth bending stress correction factors *[–]*
α_0	Normal engagement angle *[°]*
α	Force angle in yz-plane *[°]*
β	Position on the tooth root *[°]*
β_{rf1}	Position on the tooth root rounding *[°]*
γ_F	Force angle in xz-plane *[°]*
σ	Normal stress *[N/mm²]*
σ_{FG}, σ_{FP}	Stress limit and permissible stress *[N/mm²]*
σ_F, σ_{F0}	Maximum local and nominal stress *[N/mm²]*
σ_1	Maximum principal stress *[N/mm²]*
σ_{Hmax}	Maximum Hertzian contact pressure *[N/mm²]*
τ	Shear stress *[N/mm²]*
τ_{FG}	Shear stress limit *[N/mm²]*
τ_F	Maximum local shear stress *[N/mm²]*
υ_1, υ_2	Poisson ratio of worm and wheel *[–]*

Funding Open Access funding enabled and organized by Projekt DEAL.

Conflict of interest J. Gründer and A. Monz declare that they have no competing interests.

References

1. DIN 3996: Tragfähigkeitsberechnung von Zylinder-Schneckengetrieben mit sich rechtwinklig kreuzenden Achsen. 2019
2. ISO/TR 14521: Gears—Calculation of load capacity of wormgears. 2009
3. Niemann G, Winter H (1983) Maschinenelemente, 2nd edn. vol 3. Springer, Berlin Heidelberg
4. Norgauer P (2021) A new approach for the calculation of worm shaft deflection in worm and crossed helical gear drives. AGMA Technical Paper
5. Gründer J (2021) Advanced calculation of the deflection of worm shafts with FEM. IOP Conference Series: Materials Science and Engineering 1190.
6. ANSI/AGMA 6022-C93: Design Manual for Cylindrical Wormgearing. 2014
7. Dinter R (1996) Schneckentragfähigkeitsgrenzen ermitteln und erhöhen. FVA-Forschungsheft 518. Forschungsvereinigung für Antriebstechnik e. V., Frankfurt/Main
8. Rhode, A.: Riefenbildung an einsatzgehärteten Schnecken in Abhängigkeit von Belastung, Drehzahl, Baugröße, Schmierstoff, Tragbildlage und Schneckenradbronze. RU Bochum Diss. 2011
9. Lange, N.: Hoch fresstragfähige Schneckengetriebe mit Rädern aus Sphäroguss. TU München Diss. 2000
10. Thiele R (2006) Zahnfuß-Tragfähigkeitsberechnung für Schneckenräder auf Basis des Zahnfußschädigungskonzeptes. FVA-Forschungsheft 784. Forschungsvereinigung für Antriebstechnik e. V., Frankfurt/Main
11. Geuß, M.: Tragfähigkeit von Schneckengetrieben beim Einsatz von lebensmittelverträglichen Schmierstoffen mit Kontamination von Wasser. RU Bochum Diss. 2013
12. Roth P (2021) Verschleiß- und Fresstragfähigkeit von Schneckengetrieben aus höherfesten Werkstoffen bei Langsamlauf für Öl- und Fettschmierung. FVA-Forschungsheft 1459. Forschungsvereinigung für Antriebstechnik e. V., Frankfurt/Main
13. Rhode A, Wrona E (2006) Induktives Härten von Getriebeschnecken. FVA-Forschungsheft 798. Forschungsvereinigung für Antriebstechnik e. V., Frankfurt/Main
14. Michels, K.: Entwicklung eines hochbelastbaren Schneckengetriebes mit Werkstoffpaarung Stahl/Grauguss. TU München Diss. 1968
15. Sternberg M (1996) Schneckenräder aus gehärtetem Stahl. FVA-Forschungsheft 488. Forschungsvereinigung für Antriebstechnik e. V., Frankfurt/Main
16. Chmill D, Tenberge P, Klitenynikov V, Brecher C, Brimmers J, Winkel O (2016) Verbundprojekt Stahl-Schnecke – Kupfer- und zinnfreie Schneckenradgetriebe hoher Effizienz und Leistungsdichte – technologische Substitution von Bronze durch Stahl: gemeinschaftlicher Abschlussbericht. Bonfiglioli Vectron MDS
17. ISO 6336-3: Calculation of load capacity of spur and helical gears—Part 3: Calculation of tooth bending strength. 2020
18. DIN 3990-1: Tragfähigkeitsberechnung von Stirnrädern – Teil 1: Einführung und allgemeine Einflussfaktoren. 1987
19. Wächter M, Müller C, Esderts A (2021) Angewandter Festigkeitsnachweis nach FKM-Richtlinie, 2nd edn. Springer Vieweg, Wiesbaden
20. Rhode A (2009) Riefenbildung an gehärteten Schnecken. FVA-Forschungsheft 889. Forschungsvereinigung für Antriebstechnik e. V., Frankfurt/Main
21. Weisel C (2009) Schneckengetriebe-Baugrößeneinfluss: Verschleiß- und Grübchentragfähigkeit von großen Zylinder-Schneckengetrieben mit optimierter Radbronze. FVA-Forschungsheft 892. Forschungsvereinigung für Antriebstechnik e. V., Frankfurt/Main
22. Monz, A.: Tragfähigkeit und Wirkungsgrad von Schneckengetrieben bei Schmierung mit konsistenten Getriebefetten. TU München Diss. 2012
23. Heilemann, J.: Tragfähigkeit und Wirkungsgrad bei unterschiedlichen Schnecken-Zahnflankenformen unter Berücksichtigung der Oberflächenhärte und Härtetiefe. TU München Diss. 2005
24. DIN 743-2: Tragfähigkeitsberechnung von Wellen und Achsen – Teil 2: Formzahlen und Kerbwirkungszahlen. 2012
25. Elkholy AH, Falah AH (2015) Worm gearing design improvement by considering varying mesh stiffness. Int J Mech Mechatronics Eng 9(9):1647–1650
26. Sudoh K, Tanaka Y, Matsumoto S, Tozaki Y (1995) Load distribution analysis method for cylindrical worm gear teeth. Transcr Jpn Soc Mech Eng Ser C 59(566):606–613
27. Simon V (1996) Stress analysis in worm gears with ground concave worm profile. Mech Mach Theory 31(8):1121–1130
28. Pfister C, Pfister J, Kazaz L, Eberhard P (2018) Stress calculation in worm gears using elastic multibody models. The 5th Joint International Conference on Multibody System Dynamics, Lisboa
29. Litvin FL, Gonzalez-Perez I, Yukishima K, Fuentes A, Hayasaka K (2007) Design, simulation of meshing, and contact stresses for an improved worm gear drive. Mech Mach Theory 42:940–959
30. Reißmann, J.: Beitrag zur Entwicklung einer verbesserten Berechnungsmethode für die Zahnfußtragfähigkeit von Zylinderschneckengetrieben. TU Chemnitz Diss. 2016
31. Hermes, J.: Tragfähigkeit von Schneckengetrieben bei Anfahrvorgängen sowie Last- und Drehzahlkollektiven. RU Bochum Diss. 2008
32. ISO/TR 10828: Worm gears—Worm profiles and gear mesh geometry. 2015
33. Lutz, M.: Methoden zur rechnerischen Ermittlung und Optimierung von Tragbildern an Schneckengetrieben. TU München Diss. 2000
34. DIN 3990-3: Tragfähigkeitsberechnung von Stirnrädern – Teil 3: Berechnung der Zahnfußtragfähigkeit. 1987
35. Schinagl, S.: Zahnfußtragfähigkeit schrägverzahnter Stirnräder unter Berücksichtigung der Lastverteilung. TU München Diss. 2002
36. Umezawa K (1973) The meshing test on helical gears under load transmission (2nd report, the approximate formula for bending-moment distribution on gear tooth). Bull Jpn Soc Mech Eng 16(92):407–413
37. Linke H, Börner J (2023) Stirnradverzahnungen. Berechnung – Werkstoffe – Fertigung, 3rd edn. Hanser, München
38. DIN 3975: Begriffe und Bestimmungsgrößen für Zylinder-Schneckengetriebe mit sich rechtwinklig kreuzenden Achsen – Teil 1: Schnecke und Schneckenrad. 2017